BNL-220727-2020-JAAM

Using solenoid as multipurpose tool for measuring beam parameters

I. Pinayev

To be published in "Review of Scientific Instruments"

December 2020

Collider Accelerator Department

Brookhaven National Laboratory

U.S. Department of Energy

USDOE Office of Science (SC), Nuclear Physics (NP) (SC-26)

DISCLAIMER

Using solenoid as multipurpose tool for measuring beam parameters

Igor Pinayev,[1]* Yichao Jing,[1,2] Dmitry Kayran,[1,2] Vladimir N. Litvinenko,[1,2] Jun Ma[1], Kentaro Mihara,[2] Irina Petrushina,[2] Kai Shih,[2] Gang Wang,[1,2] Yuan Hui Wu[2]
[1]Collider-Accelerator Department, Brookhaven National Laboratory, Upton, NY 11973, USA
[2] Department of Physics and Astronomy, Stony Brook University, Stony Brook, NY 11794, USA

Abstract

Solenoids are frequently used for focusing low energy beams. In this paper, we show how they can serve as multipurpose diagnostics tools to measure various beam parameters, including energy, emittance, the second moments of the transverse distribution, and the beam position and angle with respect to the solenoid's axis. The energy measurement is based on rotation of the plane of the transverse motion, as opposed to generating dispersion with a dipole. Measurement of the beam trajectory with respect to the solenoid axis is done by analyzing the beam orbit downstream of the solenoid while varying its current. The second moments are calculated by analyzing the beam image on a profile monitor while accounting for the beam rotation caused by the solenoid. We describe in detail the corresponding procedures and the experimental results of these measurements.

PACS numbers: 29.27.-a, 29.27.Fh

I. INTRODUCTION

Solenoids are widely used for the low energy beams optics control. They provide focusing in both planes and preserve the axial symmetry of the system. To date, the focusing properties of the solenoids have mostly been used to measure beam emittance and β and α functions.[1-4]

On a few occasions, the full transport matrices of solenoids have been used for alignment of the beam trajectory in them to preserve beam emittance.[1,5] As described in Refs.[5-7] the beam position was measured as a function of current in the upstream solenoid. In the described cases the magnetic field of the solenoid overlaps with the electric field of the gun, which requires tracking simulations[6,7] or the use of a dedicated program (in Ref.[1], the transport matrix was calculated by using a special script[8]) to fit the measured results and to extract the beam orbit. Reference[1] gives no description of how the parameters of the beam orbit were found, whereas Reference[5] used an iterative process with successive approximations was utilized. In Ref.[9], the gun position was adjusted to minimize the beam kick from the solenoid with an iterative procedure requiring multiple scans.

We describe herein methods to measure beam energy, beam trajectory, and the transverse beam distribution by using solenoids and other common equipment [e.g. profile monitors, beam position monitors (BPMs), and steering magnets]. First, we measure the energy of the beam by using the fact that a solenoid rotates the plane of the transverse motion, and this angle is unambiguously defined by the beam rigidity and the integral of the longitudinal field in the solenoid.[10] Next, we use the solenoid for the beam-based alignment by measuring the beam trajectory (both coordinates and angles) with respect to the solenoid axis and aligning the beam trajectory with the solenoid's axis.[11] Such beam-based alignment allows us to vary solenoid focusing without affecting the beam trajectory. Propagating the beam along the solenoid axis is also important for minimizing the beam emittance.

*pinayev@bnl.gov

In our case, as well as in many others, the solenoid field does not overlap with electric fields, we use a matrix approach to describe the transverse beam displacement at the observation point (i.e. a BPM or a profile monitor) as a function of the solenoid's current. We generalized the method for an arbitrary transfer function between the solenoid and the observation point. The 4×4 transport matrix is calculated by using the already known beam energy (rigidity) and the magnetic measurement data. Finally, we use beam profile monitors and solenoid scans to measure transverse beam emittances and second moments of the transverse distribution.[12]

The procedures described above transform the solenoid into a multifunctional tool for measuring electron beam parameters. The utilized methods can be also be used to measure the properties of the other low-energy beams.

II. SOLENOID-BASED BEAM ENERGY MEASUREMENTS

Beam energy measurements commonly use a spectrometer with a large-angle dipole magnet. High accuracy implies a good knowledge of the beam trajectory prior to the dipole and of the dipole field profile. The energy spectrometer requires an additional beamline hardware, which is often a subject to space constraints. Although the proposed method avoids some of these requirements, it is subject to other limitations, which are described below.

To measure beam energy,[10] we use the rotation of the plane of the transverse motion by solenoid,[13-15] as described by

$$\theta_{rot} = \int \frac{eB_z(z)}{2pc}\,dz \tag{1}$$

This idea comes from our observation with the beam profile monitor of the rotated images of two dark-current emitters at the cathode of our superconducting RF (SRF) gun (Fig. 1). Because the reversal of the solenoid current does not change the focusing strength, it also does not change the beam image at the profile monitor but rotates (and perhaps shifts) the image by the angle

$$\Delta\theta_{rot} = \int \frac{e\left(B_z^{+}(z) - B_z^{-}(z)\right)}{2pc}\,dz \tag{2}$$

Later we found that a similar idea was studied based on images of a beam passing through a slit placed before a solenoid.[16] While good for illustrative purposes and qualitative analysis, this method based on analyzing image rotation is insufficiently accurate to be applied to regular operations.

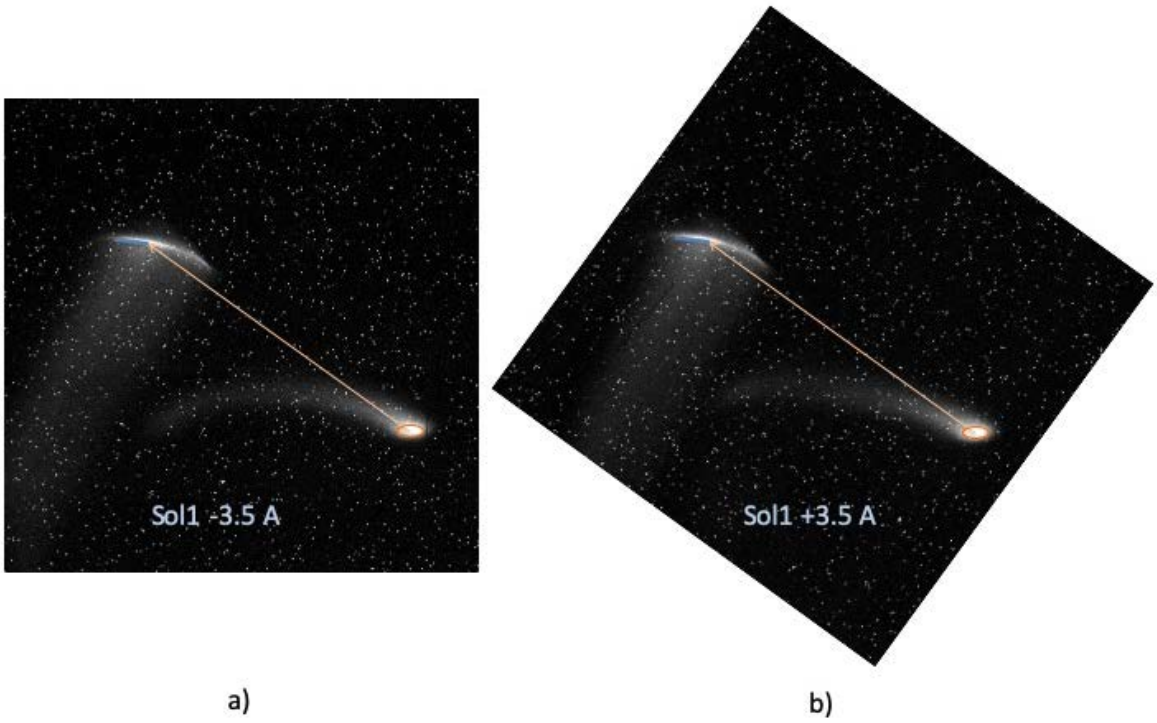

FIG. 1. Images of the dark current at profile monitor for (a) negative and (b) positive current in the solenoid Sol1 (the system layout is described in Section V). The rotation angle of 54° for the current change from –3.5 A to +3.5 A corresponds to a beam rigidity of 5.41 kGs cm and an electron momentum of 1.62 MeV/c.

For accurate measurements of the beam energy we steer the beam with the trim dipoles located upstream of the solenoid and measure the location of the beam in the XY plane at the observation point. As mentioned above, the solenoid rotates the plane of the transverse motion with the direction of the rotation (clockwise or counterclockwise) dictated by the sign of the particles charge and the direction of the solenoidal field [see Eq. (1)]. For a trim dipole steering the beam by an angle α, the change (δx, δy) of the beam position at the observation point can be found from the effective length d, which is defined by the distance between the elements and the focusing properties of the solenoid, by the rotation angle Θ by the solenoid, and by the roll angle Θ_{trim} of the trim dipole

$$\begin{pmatrix}\delta x\\ \delta y\end{pmatrix} = \alpha d \begin{pmatrix}\cos(\Theta + \Theta_{trim})\\ -\sin(\Theta + \Theta_{trim})\end{pmatrix} \tag{3}$$

With the varying corrector strength, the beam moves along a straight line in the XY plane tilted at the angle $\Theta + \Theta_{trim}$.

By using Eq. (2) and the magnetic measurement data, one can easily find the beam rigidity from the value of the Larmor rotation angle and, thus, its momentum and energy. The field integral is usually known with a high accuracy – in our case, it was measured with an accuracy better than 0.1%. Moreover, Ampere's law means that the integral of the magnetic field depends only on the enclosed current (i.e., the product of the coil current and the number of turns) and fundamental constants. Therefore, this method is affected by neither distortion of the solenoid field nor hysteresis.

To avoid systematic errors caused by the roll angle Θ_{trim} of the corrector, we use two solenoid current setpoints. We chose the setpoints corresponding to the tightly focused beam with just a sign reversal of the solenoid current.

The only uncertainty of this method is related to the rotation of the plane of oscillation by more than 360° (i.e., by one or more turns). However, this uncertainty is easily eliminated by measuring the rotation angle at a few intermediate solenoid fields.

The range of motion is limited by a few millimeters, and to ensure accuracy, the position of the beam should be measured with a precision exceeding a few microns. Using multiple measurement points reduces statistical errors and thus ensures a precise determination of the direction of motion.

Systematic errors due to the non-linearities should be on the same low level because they affect measured tilt angle. They are hard to avoid with conventional BPMs, so we base our measurements instead on the profile monitor. The rotation angle is on the order of one radian, which requires nonlinearities to be on the order of 10^{-3} or less. Using corrections can bring the nonlinearities of the BPM to a few percent, but distortion remains clearly visible.[1] Other sources of systematic errors are discussed in Section V.

Note that solenoid-based beam energy measurements do not require knowledge of the source that induces the beam displacements and do not rely on calibration of the source. The only important feature is that the direction of the kick (displacement) is constant for all settings. Thus, for guns with photocathodes, instead of using trim dipoles one can scan a laser spot over the cathode.

III. MEASUREMENT OF BEAM TRAJECTORY

To measure the beam trajectory with respect to a solenoid axis, we vary the current in the solenoid and record the beam position at a downstream device (either the profile monitor or the BPM). The transport line matrix is calculated as the product of matrices of solenoids and drifts. The matrix is evaluated for a variable current of the solenoid, where the trajectory is measured, and fixed currents of other solenoids (if any) between the location and the observation point. In our case, a transport matrix is calculated for each current setpoint by using the magnetic measurement data with the actual solenoid approximated as a series of hard-edge solenoids.[11] Since the equations of motion are fully coupled, we obtain a full 4×4 transport matrix **M**.

To accommodate for the solenoid misalignment and the offsets in the beam position measuring device, we added two fit parameters in the form of position readings when the beam is perfectly aligned with the solenoid axis. Thus, for *N* solenoid current settings, we obtain a 6×2N response matrix **R**:

$$\mathbf{R} = \begin{bmatrix} M_{11}^1 & M_{12}^1 & M_{13}^1 & M_{14}^1 & 1 & 0 \\ M_{31}^1 & M_{32}^1 & M_{33}^1 & M_{34}^1 & 0 & 1 \\ \cdots & \cdots & \cdots & \cdots & \cdots & \cdots \\ M_{11}^N & M_{12}^N & M_{13}^N & M_{14}^N & 1 & 0 \\ M_{31}^N & M_{32}^N & M_{33}^N & M_{34}^N & 0 & 1 \end{bmatrix}$$

$$\begin{pmatrix} x_1 \\ y_1 \\ \cdots \\ \cdots \\ x_N \\ y_N \end{pmatrix} = \mathbf{R} \begin{pmatrix} x_{sol} \\ x'_{sol} \\ y_{sol} \\ y'_{sol} \\ x_{BPM} \\ y_{BPM} \end{pmatrix} \tag{4}$$

obtaining the expected linear relation $\vec{V} = \mathbf{R}\vec{U}$ between the 2N position readings $\vec{V}$ as a function of six unknowns of the problem $\vec{U}$: the beam trajectory with respect to the axis of the solenoid under study, $(x_{sol}, x'_{sol}, y_{sol}, y'_{sol},)$, and two orbit offsets at the measurement point, (x_{BPM}, y_{BPM}). The beam trajectory at the location under study is then found by solving a set of linear equations.

Applying the least-squares method to the difference between the measured data and the predictions gives

$$\Phi = \left|\vec{V} - \mathbf{R}\vec{U}\right|^2 = \vec{V}^T\vec{V} - 2\vec{V}\mathbf{R}\vec{U} + \vec{U}^T(\mathbf{R}^T\mathbf{R})\vec{U} \tag{5}$$

from which one can write the "maximum-likelihood" solution as[17]

$$\vec{U} = (\mathbf{R}^T\mathbf{R})^{-1}\mathbf{R}^T\vec{V}. \tag{6}$$

Both the sensitivity to the measurement errors and the convergence of this method depend on the spectrum of the non-negative real eigenvalues of the positively defined square matrix $\mathbf{R}^T\mathbf{R}$, which makes for a very good indicator of the sensitivity of the found trajectory to measurement error. Our studies show that using measurements of either horizontal or vertical positions alone leads to significant sensitivity to errors, making it practically impossible to determine combinations of positions and angles.

Similarly, we find that, by using a quadrupole beam-based alignment, one can find accurately determine the horizontal and vertical orbit displacements with respect to the quadrupole axis. At the same time, finding the angle of the beam trajectory, while theoretically possible, is highly sensitive to measurement errors. Thus, solenoids offer the unique feature of accurately defining both the position and angle of the beam using the beam-based alignment described above. We attribute this feature to the combination of the linear dependence of the rotation angle and the quadratic dependence of the focusing strength on the magnetic field strength of the solenoid.

Given that errors in the beam position measurements have a one-to-one correspondence with the orbit measurements, the requirements for errors are much more relaxed than for the energy measurements and are on the order of 100 μm, which allows BPMs to be used for this procedure along with the profile monitors.

IV. MEASUREMENT THE SECOND MOMENTS OF TRANSVERSE DISTRIBUTION

The use of solenoids for emittance measurements is a well-known technique.[4] The situation for the beams with coupled motion requires a dedicated four-dimensional analysis. As shown in Ref.[20], nonzero cross terms can lead to the overestimates of the emittance. In the general case, Twiss parametrization is not applicable and one can use only the measurements of the second moments of the transverse distribution: $\langle x^2\rangle$, $\langle x'^2\rangle$, $\langle xx'\rangle$, $\langle y^2\rangle$, $\langle y'^2\rangle$, $\langle yy'\rangle$, $\langle xy\rangle$, $\langle xy'\rangle$, $\langle x'y\rangle$, and $\langle x'y'\rangle$ (here we assume that all the first moments are zero). The second moments can be used to calculate of the eigenemittances.[21]

The profile monitor provides three observables: $\langle x^2\rangle=\sigma_x^2$, $\langle y^2\rangle=\sigma_y^2$, and $\langle xy\rangle=\sigma_{xy}$. For the N measurements, we can write

$$\begin{pmatrix} \sigma^2_{x(1)} \\ \sigma^2_{y(1)} \\ \sigma_{xy(1)} \\ \cdots \\ \sigma^2_{x(N)} \\ \sigma^2_{y(N)} \\ \sigma_{xy(N)} \end{pmatrix} = \mathbf{S} \begin{pmatrix} \langle x^2 \rangle \\ \langle xx' \rangle \\ \langle x'^2 \rangle \\ \langle y^2 \rangle \\ \langle y'^2 \rangle \\ \langle yy' \rangle \\ \langle xy \rangle \\ \langle x'y' \rangle \\ \langle x'y \rangle \\ \langle xy' \rangle \end{pmatrix} \tag{7}$$

where **S** is a 3N×10 matrix formed from elements of the transfer matrix **M** in a manner like that used in Ref.[18]. On the left side of Eq. (7) is a column vector containing experimental observables, and on the right side are ten seconds moments of the beam distribution at the point of interest. For illustration, we show how σ_x^2 depends on the transport matrix and ten moments (we do not show **S** explicitly due to its size):

$$\sigma_x^2 = M_{11}^2\langle x^2 \rangle + 2M_{11}M_{12}\langle xx' \rangle + M_{12}^2\langle x'^2 \rangle + M_{13}^2\langle y^2 \rangle + 2M_{13}M_{14}\langle yy' \rangle + \\ + M_{14}^2\langle y'^2 \rangle + 2M_{11}M_{13}\langle xy \rangle + 2M_{12}M_{14}\langle x'y' \rangle + 2M_{11}M_{14}\langle xy' \rangle + 2M_{12}M_{13}\langle x'y \rangle \tag{8}$$

The second moments can be found by solving the system of linear equations once at least four measurements have been made. However, matrix **S** is rank deficient. No matter how many experimental points we have the matrix rank is nine. Analysis shows that this is a fundamental feature of a system containing only solenoids and drifts. Neither the transfer matrix of a solenoid[13-15] nor the transfer matrix of a drift changes the angular momentum ⟨x'y-xy'⟩. Addition of a quadrupole to the transport line can help to resolve these moments. However, given that we have no quadrupoles in the low-energy beam transport, we assume ⟨x'y⟩=⟨xy'⟩ in the analysis of the experimental results (e.g., zero angular momentum in the beam).

Note that the proposed approach is suitable for the emittance dominated beams. The substantial space charge forces will introduce systematic errors that are beyond the scope of this paper.

V. EXPERIMENTAL RESULTS

A. Experimental set-up

In our accelerator (see Fig. 3), the first dipole magnet is located after the main linac 12 m downstream of the electron gun.[19] However, performing beam low-energy measurements with this dipole, while possible, is cumbersome. At the same time, we have six solenoids between the 1.25 MV SRF gun and the 13 MV SRF linac. This motivated us to find an accurate method of using the solenoid magnets to measure the beam energy after the gun.

The CeC accelerator is equipped with numerous air-coil dipoles for the beam orbit correction. Two horizontal and two vertical orbit correctors are positioned between each pair of the solenoids, except for the closely spaced solenoids Sol4 and Sol5, which have a single corrector in each plane. This set-up allows us to correct the beam trajectory (both positions and angles) in Sol2-Sol4 and the beam position in Sol5. To achieve good accuracy, we used magnetic measurements data for each of our solenoids. All our solenoids are fed by the individual bipolar power supplies and we use this feature to measure the beam parameters. The electron beam is accelerated by the 13.1

MeV 704 MHz SRF linac, which is followed by a matching section with three quadrupoles, BPM3 and a 45° bending magnet beam line (dogleg) with three quadrupoles, BPM4, and the profile monitor YAG4. The rest of the beamline (including the full power beam dump) is not relevant to this discussion and is omitted from the description. When the dipole magnet is turned off, the beam propagates straight to the low-power beam dump and can be intercepted by the profile monitor YAG3.

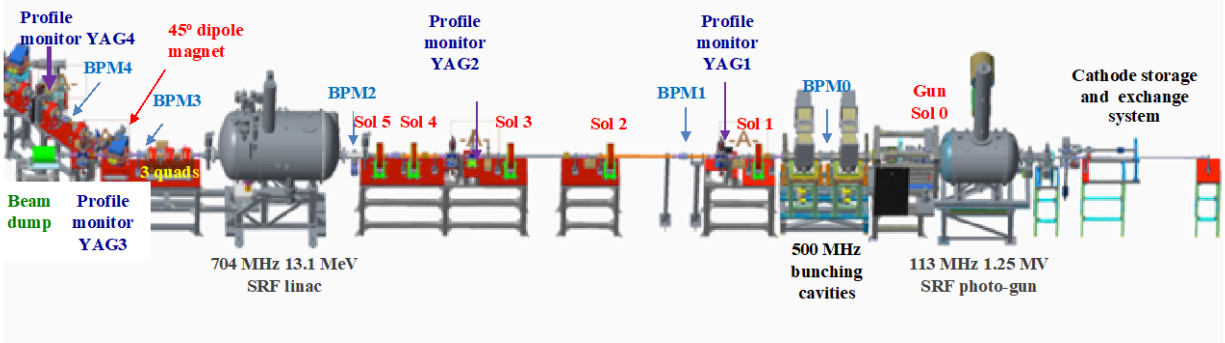

FIG. 2. Layout of CeC accelerator. From right to left: the 1.25 MeV 113 MHz SRF gun system, the low-energy beam transport (LEBT) line equipped with the six solenoids (gun Sol0, LEBT Sol1–Sol5), two 500 MHz room-temperature bunching RF cavities, three beam position monitors (BPM0–BPM2), and two profile monitors (YAG1 and YAG2),

B. Energy measurement

We tested the proposed technique by using either profile monitors or the BPMs to measure the beam position at each setting. Using the profile monitors allows us to use a relatively low charge per bunch and a well-focused beam spot. Images generated at YAG crystals were digitized by CCD cameras and analyzed to determine the center of gravity of the beam. We found that the profile monitor is very linear and scales well (i.e., it does not introduce non-linear distortions). In addition, the profile monitor has the advantage of allowing us to visually inspect images to ensure that they are well inside the area of the YAG crystal. The shape and intensity of the beam spot are stable during the measurements and, since we measure the center of gravity, no strict requirements are imposed on the YAG or camera resolution. The statistical noise in the beam position measurement with the profile monitor is 30-40 μm.

In contrast, the use of the BPM introduces significant linear and nonlinear distortions. We observed a substantial difference – as high as 30% – in the change of the tilt angles when using vertical and horizontal trims. This effect is especially noticeable for large changes in orbit or/and large beam sizes. The reduction of scanning range degrades the BPM signal-to-noise more ratio and degrades the measurement precision. These challenges could be specific to our BPM system (we have a substantial signal loss in one of the channels), so this result should not be interpreted to mean that BPMs cannot be used for such a task.

The measurements were made using an automated MATLAB script. The operator would choose a diagnostic suite consisting of a profile monitor, an upstream solenoid with its current setpoints, a set of horizontal and vertical dipole trims, a number of setpoints for the trim current and their middle current settings, and the scan amplitude. We typically used the profile monitor YAG1 and solenoid Sol1 for the measurements. To avoid saturating the camera, the measurements were made with a 20-30 pC beam charge, which is well below the operational level of 1 nC.

The script performs two current scans in each of the dipole trims for the two settings of the solenoid magnet. The code then calculates the tilt angles of the fitted lines and extracts the rotation angle caused by the solenoid. Finally, the rigidity of the electron beam and its kinetic energy are calculated. Figure 3 shows a scan using the YAG1 profile monitor, with the Sol1 solenoid excited by ±4.1A current and two upstream orbit correctors (*inj.tv2* and *inj.th2*), with a middle setting I_{co} and current range I_r.

During the scans, the current of each trim was stepped from I_{co}–I_r to I_{co}+I_r with short pauses for measuring the beam position at the YAG screen. At the end of the scan, the current of each trim was returned to its initial value prior to the scan. The same procedure was repeated for the opposite sign of the solenoid current (or just another current setting). The range of the current settings for the trim can be chosen differently for each scan to compensate for steering by the solenoid.

As shown in Fig. 3, the measured points fit closely along straight lines – this is the main advantage of using a profile monitor with a CCD camera and small-angle optics. The measurements shown were made, after the beam trajectory was set on the solenoid axis, by using the technique described in Section V. This allows the range of trim currents to be the same for both solenoid settings, so that the four lines cross almost at the same point.

Note that the horizontal and vertical trim scans have 2.5° and 2.6° offsets, respectively, which means that the tilts for positive and negative solenoid currents do not have the same deviation angle with respect to the *X* and *Y* axes. These offsets originate from alignment (roll) errors in the dipole trims and/or CCD camera and would constitute significant systematic error if one relied on a single measurement. However, taking the difference between the tilting angles for the two solenoid settings eliminates this systematic error.

The use of both horizontal and vertical trims suppresses other systematic errors: calibration errors of the *X* and *Y* planes and of gradient components in the stray magnetic fields. Both of them contribute to the change in the observed tilt angles. If the scale for the *X* plane differs from that for the Y plane, the measured changes in tilt will differ for horizontal and vertical trims. Such scaling errors could occur due to camera tilt; for example, a 5° deviation of the view axis from the normal to the screen gives a 0.4% error in scale. Similarly, the quadrupole component of the stray magnetic field, while focusing in one plane and defocusing in the orthogonal plane, will also provide for the difference in the tilt angles. The error due to the stray quadrupole component can be estimated as $GL/B\rho$, where G is the integrated quadrupole gradient, L is the distance from the solenoid to the profile monitor, and $B\rho$ is beam rigidity. Taking an average of the two trim scans eliminates the linear part of the dependencies. This script is used routinely to the monitor the beam energy in the injector beamline.

The accuracy of the measurements is determined by the accuracy of the magnetic measurements and solenoid power supply performance. We compared our energy measurements by using solenoids with the 45° magnet spectrometer (with the linac turned off) and found them to be consistent: the difference did not exceed ±0.1%.

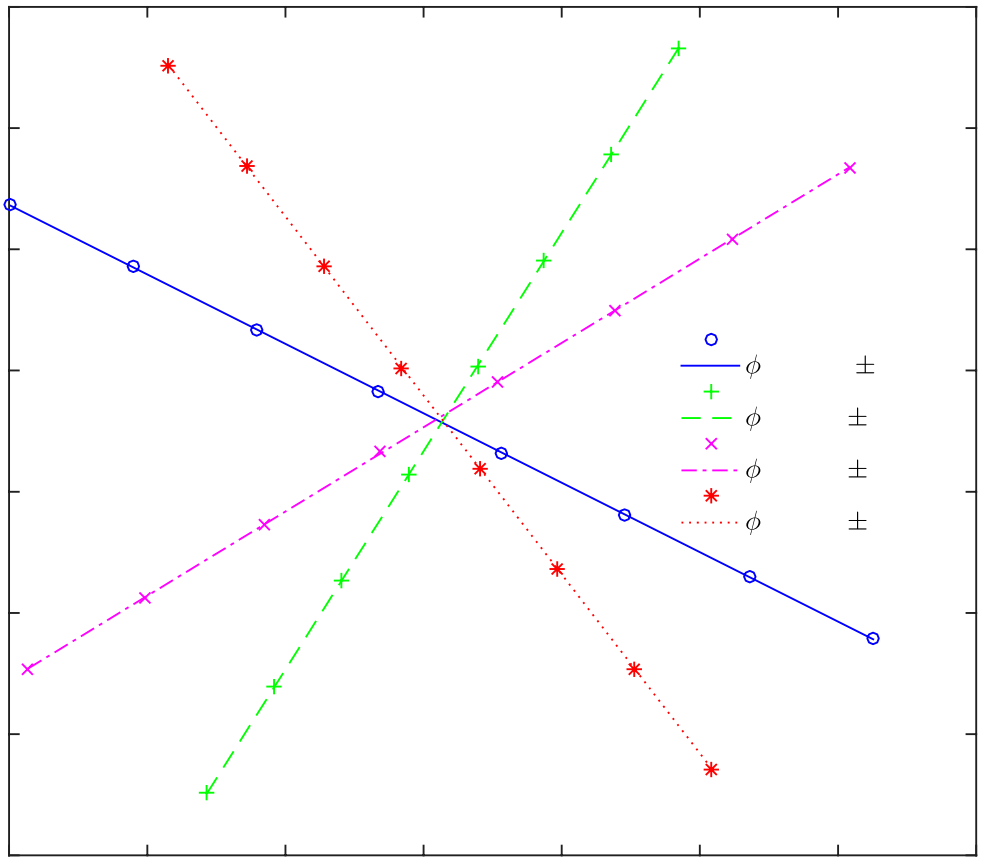

FIG. 3. Energy measurement using YAG1 profile monitor, Sol1 solenoid, and two trim dipoles (vertical inj.tv2 and horizontal inj.th2). Two sets of data show the measured beam positions during the scans of the trims (red stars for the vertical and magenta crosses for the horizontal) for a solenoid current of +4.1 A. Similarly, the set of the green pluses and blue circles show the measured beam positions for the scans at the solenoid current of –4.1 A. The corresponding lines are fits to the measured beam positions, and their tilts are evaluated. The measured angles between the two scans with the opposite solenoid polarities are 64.64±0.084° and 63.15±0.032° for the horizonal and vertical trims, respectively. The corresponding beam kinetic energy is 1.176±0.0008 MeV/c, and the beam rigidity is 5.358±0.0037 kGs cm. We consistently observe less rotation when using vertical trim, which we suspect is due to the quadrupole component in the stray field of the adjacent ion pump. Near the beam pipe, the stray field is on the order of tenths of Gauss.

We also tested the feasibility of the energy measurement by steering the laser spot over the cathode of the SRF gun. We have a set of two orthogonal translation stages to align the laser beam, and both were used for the beam energy measurement for the reasons described above. Rotation of the plane of motion was induced by the gun solenoid focusing the beam on the first profile monitor. Solenoid Sol1 was turned off and the rotation caused by the gun solenoid Sol0 was

measured. Fig. 4 shows the experimental results, which were confirmed with the measurements made using trims.

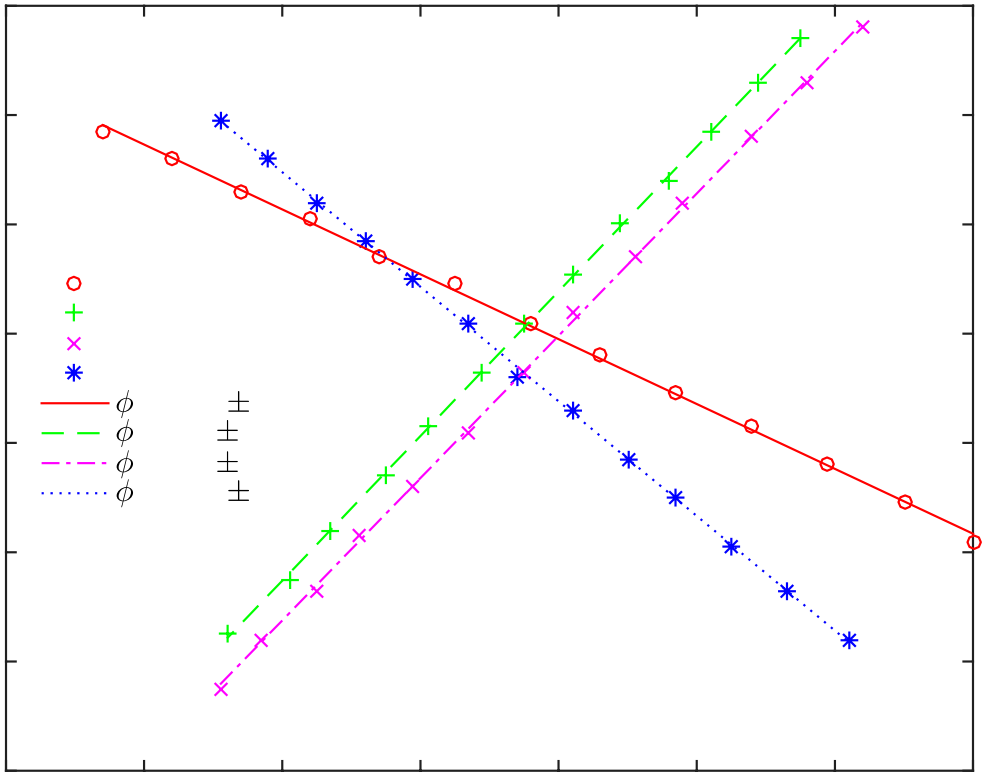

FIG. 4. Measurement of electron beam energy from electron gun made by scanning the laser spot over the cathode. The axial field integral for 8.5 A is 8.01 kGs cm. For the vertical horizontal) scan the total rotation angle is 80.7° (83.2°) (again, the change in tilt for the vertical scan is less than that for the horizontal scan). The corresponding beam kinetic energy is 1.246 MeV (these measurements were made under different conditions than those reported in Fig. 3).

Another advantage of the proposed method is insensitivity to energy spread. The measurements are based on the paraxial beam motion, and no dispersion is generated. This important feature allows us to benchmark the phase and tune the photocathode's drive laser, SRF gun and bunching cavities. Figure 5 illustrates such a measurement of the gun on-crest phase and voltage, and Fig. 6 shows the voltage and zero-crossing phase for the bunching cavities.

To phase the laser and the gun the script measures the energy of the electron beam as a function of laser phase with de-energized bunching cavities. Zero (maximal field) launching (laser) phase of the electrons at the photocathode does not correspond to the maximum energy gain – in our case, for a 1.25 MV gun voltage, the launching phase for the maximum energy gain is –15.4°. This is what we call an "on-crest" phase for the electron beam and its value of –0.23° is shown in Fig. 5.

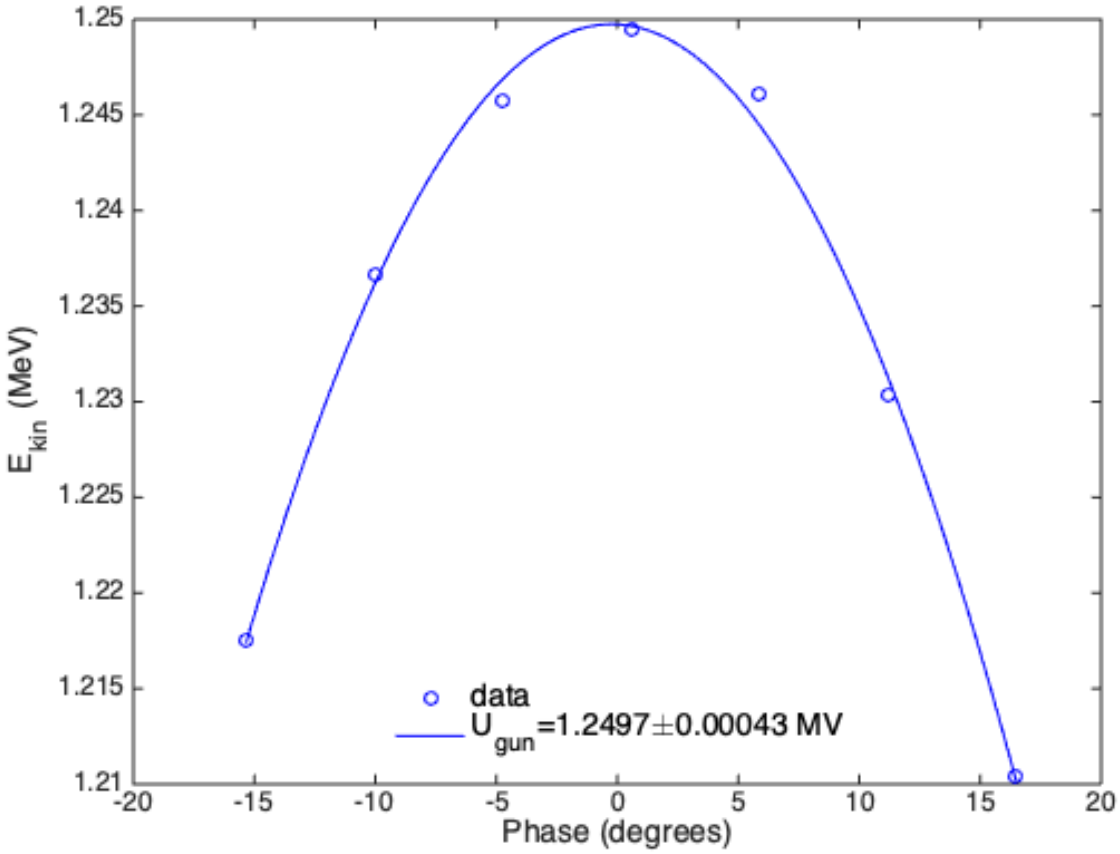

FIG. 5. Solenoid-based measurements of the 113 MHz SRF gun accelerating voltage (1.25 MV) as a function of phase. The on-crest laser phase (-0.23°) and the corresponding gun voltage are found from the parabolic fit.

After completing the first measurement, the laser phase is set to the measured "on-crest" value, the 500 MHz RF cavities are turned on and a 360° phase scan is done with 30° steps. Measured beam kinetic energies are then fit using $E = E_{gun} + \Delta E \sin(\varphi - \varphi_0)$, where φ_0 is the zero-crossing phase, E_{gun} is the beam kinetic energy from the gun (just another measurement of a known value), and ΔE is the on-crest average energy gain in the bunching cavities. When the distance between the 500 MHz cavities and the SRF gun is about 3 m, the beam is only slightly relativistic and the arrival time to the bunching cavities depends strongly on the gun voltage and phase. This makes this measurement vital for properly configuring the accelerator. Insensitivity of the method to the energy spread is very important for the above measurements: the maximum induced energy spread of the measurement shown in Fig. 6 is about 4%. Nevertheless, the obtained data obtained are well fit, which allows a precise calculation of the cavity voltage and phase.

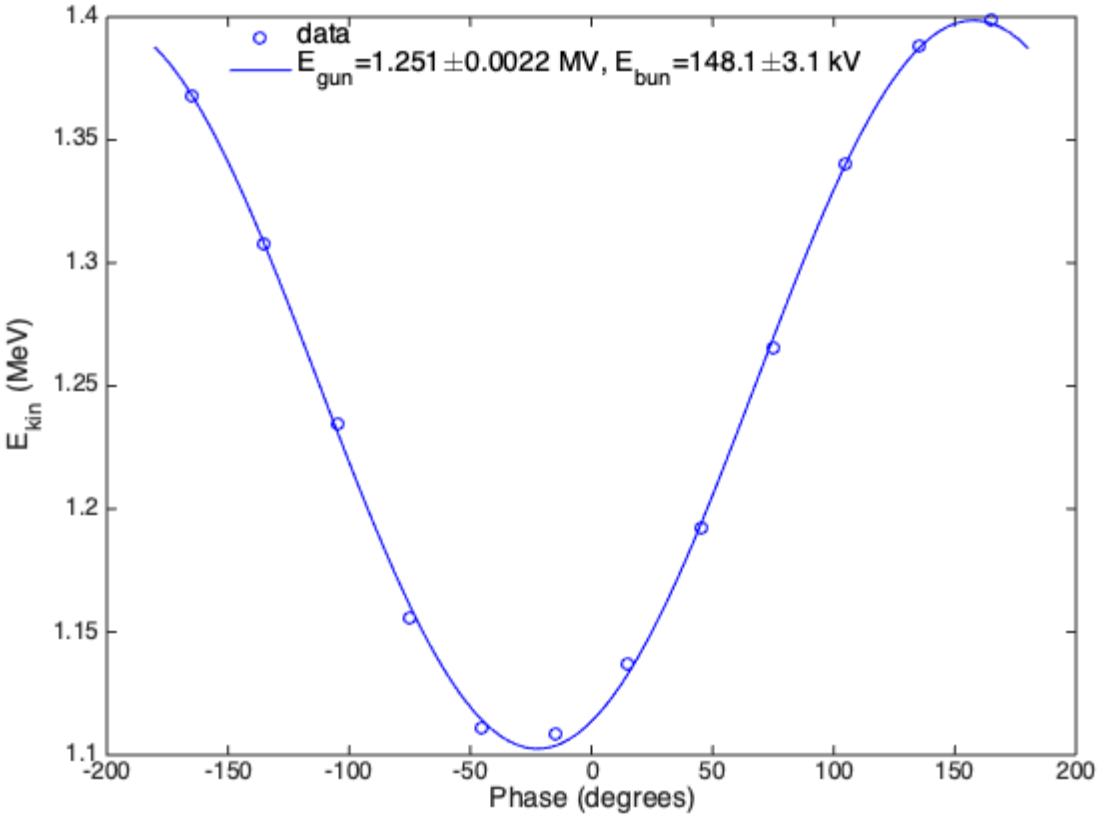

FIG. 6. Solenoid-based measurements of the voltage (157.0 kV) and the zero-crossing phase (67.7±1.2°) for the 500 MHz bunching cavities and 375 ps bunch. The voltage of the bunching cavities is greater than the displayed energy gain due to the final bunch length. Note that the phases are not absolute and correspond to the phases in the CeC accelerator low-level RF control system.

The proposed method measures the average beam energy and, so one should account for the final bunch length to properly calculate the cavity voltage. The relation between the average energy gain ΔE and the acceleration voltage of the bunching cavities depends on the longitudinal bunch shape. We used bunches with a flat-top distribution and with duration τ varying from 100 to 500 ps. For a beam with the initial kinetic energy E_0 passing through a cavity with the voltage U_{cav} and angular frequency ω the average energy as a function of phase φ is

$$\langle E\rangle = \frac{1}{\tau}\int_{-\tau/2}^{\tau/2}(E_0 + eU_{cav}\cos(\omega t+\varphi))dt = E_0 + eU_{cav}\cos\varphi\,\frac{2\sin\omega\tau/2}{\omega\tau} \qquad (9)$$

For 500-ps long bunches and 500 MHz RF frequency, the correction $\mathrm{sinc}(\omega\tau/2) = 0.9$ becomes substantial.

For a Gaussian bunch with root-mean-square duration of σ_τ, the correction coefficient can be found from

$$\langle E\rangle = \frac{1}{\sqrt{2\pi}\sigma_\tau}\int_{-\infty}^{\infty} e^{-\frac{t^2}{2\sigma_\tau^2}}(E_0 + eU_{cav}\cos(\omega t+\varphi))dt = E_0 + eU_{cav}\cos\varphi\, e^{-\frac{\omega^2\sigma_\tau^2}{2}}. \qquad (10)$$

We validated the voltage calibration and phase of the bunching cavities by setting the voltage to 63.8 kV and the phase to –90° from the zero crossing and then propagating the electron beam to the dogleg YAG4 with the linac off. These settings should compensate for the energy spread of the beam created by the time dependence of the accelerating voltage in the 113 MHz SRF gun. The minimal energy spread occurs when the electron beam is in phase with the 500 MHz valley (maximal deceleration) with the voltage inversely proportional to the square of the ratio of two frequencies. This method, which is accurate to within 0.25º and 0.1 kV, confirms the results obtained.

C. Trajectory measurement

The real-time MATLAB application is used for the solenoid beam-based alignment. The script executes the solenoid current scan (with equal steps from I_{sol}-I_{range} to I_{sol}+I_{range}, where I_{range} is the requested scan range around I_{sol}) – in the cases shown in Fig. 7, the scan is done for Sol1. At each step, the transverse position is measured (in the case of Fig. 7, it is measured by the BPM1) after a brief pause required to complete the transient processes in the solenoid power supply and update the position data. At the end of the scan, the application forms the response matrix (4) and calculates the displayed beam trajectory in the solenoid. Recall that the procedure requires only knowledge of the 4×4 transport matrix from the solenoid under test to the BPM, with the transport channel typically including from one to three solenoids. The data from all scans can be saved for later analysis or for use by other applications.

We tested the accuracy of the measurement by using the horizontal trim to introduce a calibrated angular kick in front of the solenoid. The results of this test, listed in Table I, are consistent. Modifying the horizontal angle of the beam trajectory in front of the solenoid by 14 mrad leads to a measured change of 14.9 mrad in the horizontal angle and of 1 mrad in the vertical angle. The 7% difference between the measured and introduced horizontal angle is related either to the calibration errors in the BPM or to the nonlinearity of the beam transport for large (15 mrad) angles. The measured change in the vertical plane is likely originates from the roll angle of the used trim.

TABLE I. Results of the solenoid BBA procedure test with the beam

I_{trim}, A	Trim kick, mrad	Measured x', mrad	Measured y', mrad
-2.6	10.1	0.23	4.09
0.0	0.0	-10.59	3.29
1.0	-3.9	-14.69	3.05

While imperfect, this test clearly demonstrates that the beam-based alignment using solenoids functions and provides converging results. In other words, each solenoid in our beamline could serve as two beam-position measuring devices to fully determine the beam trajectory at their location. The data obtained can be used to correct the solenoid alignment, including position and tilt angles, which is especially important to obtain the best emittance with the gun solenoids.

After verifying the accuracy of our solenoid-based trajectory measurements, the above procedure was routinely used to measure and correct the orbit. We chose to steer the beam because of mechanical constraints on the gun solenoid and substantial nonconstant stray magnetic fields from the adjacent RHIC dipoles. The initial trajectory in each of the LEBT solenoids is measured and then corrected by using four trim dipoles (two horizontal and two vertical) upstream of the

solenoid but downstream of the previous solenoid. Starting from the Sol1, we correct the beam trajectory in all solenoids except Sol5, where we can only use a single corrector for each plane and are thus able to correct only beam positions but not the angles. Figure 7 shows an example of the application of this orbit-correction method for the Sol1 magnet. This alignment is especially useful for the operations because it allows us to change the focusing properties of the low-energy beam transport without affecting the beam orbit.

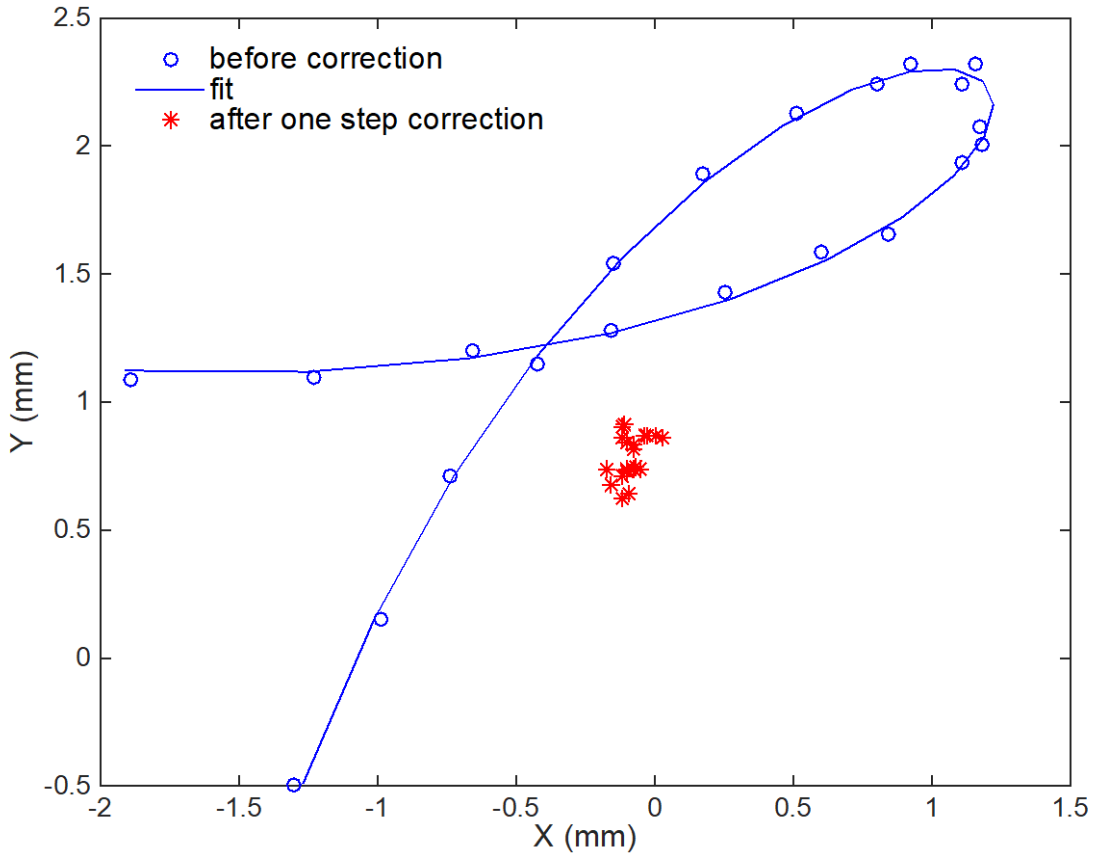

FIG. 7. Example of orbit correction in Solenoid 1 of the LEBT using BPM1 for position measurements. The graph shows the initial beam positions during the solenoid scan from -4.0 A to +4.0 A, the curve for the calculated fit coefficients, and the beam positions after applying corrections during the solenoid scan with the same parameters. The beam trajectory vs the solenoid axis prior to correction was x = 3.16 mm, y = 2.14 mm, x′ = –2.81 mrad, and y′ = –1.19 mrad. After correction, the trajectory becomes x = –0.08 mm, y = –0.26 mm, x′ = 0.01 mrad, and y′ = 0.27 mrad. The spread of measured points after correction is typical of jitter in the BPM position measurements.[19]

D. Emittance and second moments of distribution measurement

The proposed approach was tested at the CeC accelerator and used an electron beam generated by the 1.25 MeV superconducting RF gun. The bunch length was 375 ps and the bunch charge

was 0.6 nC. Figure 8 shows the measurements results. This beam is close to round (for the perfectly round beam $\sigma_x^2 = \sigma_y^2$, $\sigma_{x'}^2 = \sigma_{y'}^2$, $\sigma_{xx'} = \sigma_{yy'}$, and $\sigma_{xy} = \sigma_{x'y} = \sigma_{xy'} = \sigma_{x'y'} = 0$).

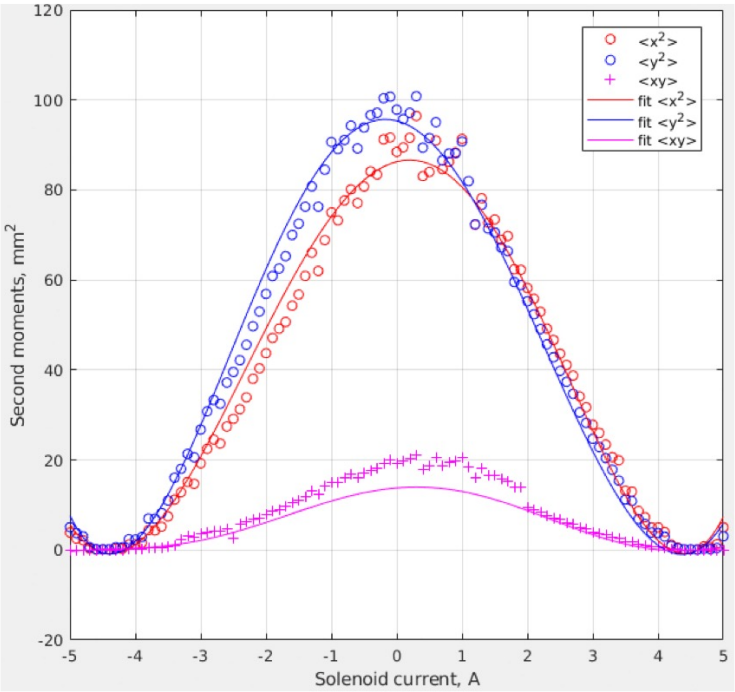

FIG. 8. Partial screenshot of the application for measurement of second moments of 1.2 MeV electron beam distribution in the CeC accelerator with solenoid and screen placed 0.61 m downstream. The found second moments are: $\langle x^2 \rangle$ = 16.8 mm^2, $\langle xx' \rangle$ = 29.9 mm mrad, $\langle x'^2 \rangle$ = 52.6 mrad^2, $\langle y^2 \rangle$ = 15.1 mm^2, $\langle yy' \rangle$ = 26.4 mm mrad, $\langle y'^2 \rangle$ = 45.6 mrad^2, $\langle xy \rangle$ = 2.3 mm^2, $\langle x'y' \rangle$ = 7.9 mrad^2, and $\langle x'y \rangle$ = $\langle xy' \rangle$ = 4.0 mm mrad.

VI. CONCLUSIONS

We demonstrate in this work that solenoid – in combination with other beamline elements – can serve as multipurpose tool to measure beam momentum and beam energy, the beam trajectory in solenoid (both positions and angles), and the second moments of the beam transverse distribution.

The methods proposed provide highly accurate measurements and evaluation of various accelerator structures. We report experimental tests of these methods for accelerator applications: from determining parameters (such as voltage and phase) of accelerator structures to beam trajectory (including position and angle) measurement and correction.

We also demonstrate that the proposed methods are robust and do not require a large charge per bunch when used with YAG screens. The methods are also tolerant to the large energy spread in beam. Given that solenoids and profile monitors make up part of typical low-energy beamlines, in most cases, the proposed methods would not require any additional equipment. These systems can also be very compact, down to 0.5 m long.

We were pleasantly surprised that linear optics provides a sufficient basis for all these techniques to be both accurate and robust. In comparison with tracking codes and the multiple iterations required for convergence to the measurement data, the proposed methods are simple,

fast, and reliable Furthermore, these measurements of energy and trajectory require no knowledge of transverse beam distribution, which would be critically important for any nonlinear tracking and for comparison with experimental results.

DATA AVAILABILITY STATEMENT

The data that support the findings of this study are available from the corresponding author upon reasonable request.

ACKNOWLEDGMENTS

The authors would like to thank T. Miller and D. Gassner (BNL) for developing and commissioning high-precision profile monitor diagnostics, Dr. T. Roser (BNL) for encouragement and continuous support of this program, and Dr. P. Thieberger for help in preparation of the manuscript.

This research was supported by DOE NP office grant DE- FOA-0000632, NSF grant PHY-1415252, and by Brookhaven Science Associates, LLC under Contract No. DE-SC0012704 with the U.S. Department of Energy.

REFERENCES

[1]C. Gulliford, A. Bartnik, I. Bazarov, L. Cultrera, J. Dobbins, B. Dunham, F. Gonzalez, S. Karkare, H. Lee, H.Li, Y. Li, X. Liu, J. Maxson, C. Nguyen, K. Smolenski, and Zhi Zhao, Phys. Rev. ST Accel. Beams, **16**, 073401 (2013).

[2]W.S. Graves, L.F. DiMauro, R. Heese, E.D. Johnson, J. Rose, J. Rudati, T. Shaftan, B. Sheehy, L/-H. Yu, and D.H. Dowell, in *Proceedings of the 2001 Particle Accelerator Conference PAC'01, Chicago, USA,* (2001), WPAH060, pp. 2230-2232.

[3]I. Bazarov, L. Cultrera, A. Bartnik, B. Dunham, S. Karkare, Y. Li, X. Liu,.J. Maxson, and W. Roussel, Appl. Phys. Lett. 98, 224101 (2011).

[4]K. Mihara, V.N. Litvinenko, D. Kayran, I. Pinayev, T. Miller, in *Proceedings of the International Particle Accelerator Conference IPAC'17, Copenhagen, Denmark,* (2017), THPAB087, pp. 3921-3923.

[5]M. Krasilnikov, J. Bahr, H.-J. Grabosch, J.H. Han, V. Miltchev, A. Oppelt, B. Petrosyan, L. Staykov, F. Stephan, M.V. Hartrott,, in *Proceedings of the 2005 Particle Accelerator Conference PAC'05, Knoxville, USA,* (2005), WPAP005, pp. 967-969.

[6]R. Cee, W. Beinhauer, W. Koch, M. Krassilnikov, A. Novokhatski, S. Ratschow, T. Weiland, P. Castro, S. Schreiber, in *Proceedings of the 2001 Particle Accelerator Conference PAC'01, Chicago, USA,* (2001), RPAH105, pp. 3096-3098.

[7]M. Krasilnikov, W. Beinhauer, R. Cee, W. Koch, A. Novokhatski, S. Ratschow, T. Weiland, P. Castro, S. Schreiber, in *Proceedings of the 2001 Particle Accelerator Conference PAC'01, Chicago, USA,* (2001), RPAH106, pp. 3099-3101.

[8]C. Gulliford and I. Bazarov, Phys. Rev. ST Accel. Beams, **15**, 024002 (2012).

[9]J. Park, M. Babzien, K. Kusche, and V. Yakimenko, in *Proceedings of the 2008 Free Electron Lasers Conference FEL08, Gyeongju, Korea,* (2008), TUPPH008, pp. 247-250.

[10]I. Pinayev, D. Kayran, V.N. Litvinenko, G. Wang, in *Proceedings of the 6th International Beam Instrumentation Conference IBIC2017, Grand Rapids, USA,* (2017), MOPCC05, pp. 47-49.

[11]I. Pinayev, Y. Jing, D. Kayran, V.N. Litvinenko, I. Petrushina, K. Shih, G. Wang, in *Proceedings of the 6th International Beam Instrumentation Conference IBIC2017, Grand Rapids, USA*, (2017), MOPCC06, pp. 50-51.
[12]I. Pinayev, in *Proceedings of the 8th International Beam Instrumentation Conference IBIC2019*, Malmo, Sweden, (2019), WEPP042.
[13]R. Larsen, Spear-107, 1971.
[14]S.Y. Lee, *Accelerator Physics* (World Scientific, Singapore, 1999), p. 180.
[15]H. Wiedemann, *Particle Accelerator Physics II* (Springer, Berlin, 2003), pp. 83-86.
[16]S.Q. Liao, Ch. Cheng, S.X. Zheng, Ch.X. Tang, Yu.Z. Lin, X.B. Ling, F. Mu, H.F. Pang, Beam characterizations of the Mini-LIA, in *Proceedings 17th International Conference on High Power Particle Beams*, Xian, China (2008) pp. 390-391, 2008.
[17]A. Charnes, E.L. Frome, P.L. Yu, J. Am. Stat. Assoc. **71** (1976), pp. 169–171.
[18]M.G. Minty and F. Zimmerman, *Measurement and Control of Charged Particle Beams* (Springer, Berlin, 2003), pp. 104-106.
[19]I. Pinayev, Z. Altinbas, J.C. Brutus, A. Curcio, A. DiLieto, T. Hayes, R. Hulsart, P. Inacker, Y. Jing, V.N. Litvinenko, J. Ma, G. Mahler, M. Mapes, K. Mernick, K. Mihara, T. Miller, M. Minty, G. Narayan, I. Petrushina, F. Severino, K. Shih, Z. Sorrell, J. Tuozzolo, E. Wang, G. Wang, and A. Zaltsman in *Proceedings of 10th International Particle Accelerator Conference IPAC'19*, Melbourne, Australia, (2019), MOPMP050, pp. 559-561.
[20]L. Zheng, J. Shao, Y. Du, J.G. Power, E.E. Wisniewski, W. Liu, C.E. Whiteford, M. Conde, S. Doran, C. Jing, C. Tang, and W. Gai, Phys. Rev. ST Accel. Beams, **21**, 122803 (2018)
[21]C. Xiao, O. K. Kester, L. Groening, H. Leibrock, M. Maier, and P. Rottlander, Phys. Rev. ST Accel. Beams, **16**, 044201 (2013)